First-principles analysis of the STM image heights of styrene on Si(100)

K. H. Bevan,[1,*] F. Zahid,[2] D. Kienle,[3] and H. Guo[2]
[1]*NSF Network for Computational Nanotechnology, Purdue University, West Lafayette, Indiana 47907, USA*
[2]*Centre for the Physics of Materials and Department of Physics, McGill University, Montreal PQ, Canada H3A 2T8*
[3]*Sandia National Laboratories, Livermore, California 94550, USA*
(Received 30 January 2007; revised manuscript received 17 April 2007; published 23 July 2007)

We report on theoretical investigations of scanning tunneling spectroscopy (STM) image heights on Si(100). Calculations are performed using density functional theory (DFT) within the Keldysh nonequilibrium Green's function (NEGF) formalism. The nonequilibrium potential drop between Si(100) and a STM tip is determined self-consistently. This potential drop is found to play an important role in the calculated image height characteristics of adsorbed hydrocarbons by lowering the vacuum barrier and shifting molecular levels. Numerical data collected for image heights of styrene against a hydrogen passivated Si(100) background are found to agree quantitatively with the corresponding experimental results. We also present a comparison between results obtained by the NEGF-DFT formalism and the Tersoff-Hamann approximation, showing that nonequilibrium analysis can be important in the study of STM image heights of molecules.

DOI: 10.1103/PhysRevB.76.045325 PACS number(s): 73.22.−f, 73.40.−c, 68.37.Ef, 71.15.−m

I. INTRODUCTION

As technology continues to advance towards atomic dimensions, the scanning tunneling microscope (STM) is increasingly utilized in the study of devices on this scale. Various effects including radiative emission, negative differential resistance, switching, and charge regulation have been observed at atomic dimensions.[1–5] There is a strong need to characterize distance-dependent bonding properties between a protodevice and a STM tip during current-voltage measurements.[6] This is necessary for properly evaluating device performance since STM current measurements can differ by several orders of magnitude depending on the distance between the tip and sample. On semiconductor surfaces such as a silicon surface, this is, however, a rather complicated task due to effects such as surface reconstruction, band bending, self-consistent electronic level corrections to molecular adsorbates, and the polarization of surface states by an applied electric field. All these effects influence STM measurements and data interpretation.[7,9–11] A detailed understanding of atomic contact properties is required as one pushes towards more exotic devices interfaced with silicon.[2,3,5]

STM height and current-voltage measurements on Si(100) that have been reported extensively in the literature for many years include a broad range of hydrocarbons such as C_2H_4, C_2H_2, styrene, benzene, diphenyl, and cyclopentene.[2,5,6,12–18] In many cases a molecular sample appears only as a fraction of its geometric height above the substrate (in the STM image). In other instances the sample can even appear darker than the substrate[12,15] which can be misinterpreted to imply that the sample is located inside the substrate. It is also not always clear what role is played by the applied bias in a STM measurement. These and other puzzles have led to many useful theoretical investigations of STM image height characteristics.

Most recently, Hückel-based modeling of styrene on Si has been reported,[16] with an emphasis on lateral transport, heights, and methyl end groups. The bias dependence of styrene image heights and tip sample interaction have also been of interest, particularly with a lack of explanation for the negative heights arising at lower imaging voltages.[15] As well, height simulations of C_2H_2 and C_2H_4 contrast inversion have uncovered noticeable contributions due to surface polarization on clean Si(100).[7,14] Polarization by an applied electric field extends clean Si(100) dimer states into the vacuum to such an extent that their measured profile height lies above that of adsorbed C_2H_4 molecules under certain bias conditions. Smaller hydrocarbons such as C_2H_4 remain closely attached to the surface and are therefore only lightly affected by the applied bias. However, due to its small height, the molecule can appear smaller than nearby clean silicon dimers which undergo slight polarization under an applied electric field. This polarization raises the STM height profile of the clean substrate by approximately 0.5 Å (Ref. 8) and is therefore an issue for short molecules but not that critical to interpreting the height features of longer molecules such as styrene. These effects are limited to clean silicon surfaces. Finally, the relative equilibrium energetic position of occupied surface states was shown to influence STM heights.[19] Due to the immense importance of interpreting STM height data, further investigations of STM image heights on Si(100) are warranted. In particular, we note that previous atomistic studies of this problem were based on calculating the electronic structure of the tip and substrate *separately* and at equilibrium.[15] On the other hand, when current flows from the STM tip into the substrate, the problem is inherently nonequilibrium and in principle the atomic potentials should be determined under nonequilibrium conditions. It is the purpose of this study to carry out such nonequilibrium calculations.

Our work is concerned with passivated Si(100). We address three open questions regarding molecular STM height measurements on passivated Si(100): what is the role of electrostatics, what is the role of the substrate band gap, and is a nonequilibrium model required to obtain results that explain experimental data quantitatively? In this context we examine the experimentally well-studied system of styrene adsorbed on hydrogen-passivated Si(100). A subtle interplay between tip-sample electrostatics and surface band structure is shown to strongly influence STM height measurements. The importance of applying the self-consistent nonequilibrium Green's function (NEGF) method[20,21] under high bias is highlighted.

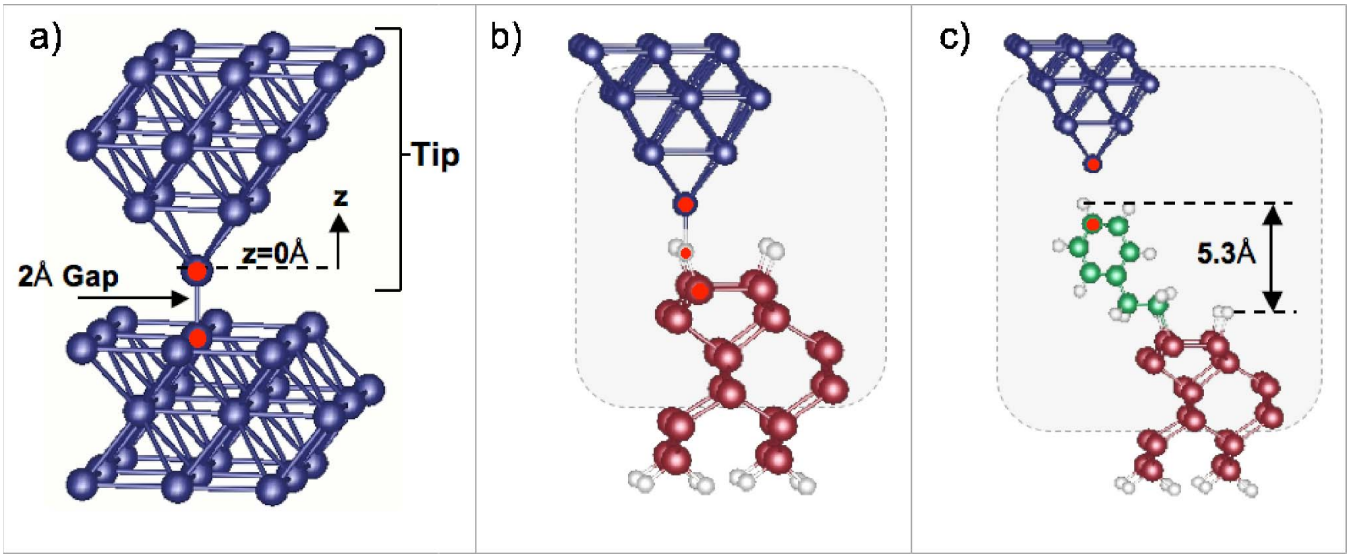

FIG. 1. (Color online) Atomic geometry of the tip-sample system. The structures are obtained by DFT total energy relaxation. (a) Al(100)-(3×3) tip and Al substrate structure. The same tip is placed above all Si(100) substrates. (b) Al tip on a Si(100)-(2×1) passivated and reconstructed surface. (c) Al tip on a Si(100)-(2×1) styrene surface. To reduce computation, the styrene unit cell includes one styrene molecule from the relaxed geometry of an infinite (periodic) styrene chain. Within the LDA, the optimized geometric height of styrene against a Si(100) passivated background is 5.3 Å. The solid circles indicate the position of free atomic orbitals used for $I(z)$ calculation (see Sec. III C). The shaded gray area indicates the subset of atoms that form the scattering region of two-probe transport analysis by NEGF.

As one of the longer hydrocarbons studied extensively on silicon, styrene resides close to the STM tip even at substantial bias voltages and low imaging currents (−3 V, 50 pA).[15] Under these STM imaging conditions styrene is subjected to a large voltage drop which shifts its energy levels, thereby affecting its height characteristics. On the other hand, at low bias it is the Si-substrate band gap that dominates transmission. We are able to attribute the experimentally observed negative styrene STM heights at (−1.5 V, 50 pA) (Ref. 15) to low transmission at the edges of the Si(100) band gap. Finally, we compare the NEGF results with that obtained by the Tersoff-Hamann approximation.[22,23]

The remainder of the paper is organized into five subsequent sections. Section II discusses the geometry under investigation. The *ab initio* NEGF method and other calculation details are outlined in Sec. III. In Sec. IV we present current-voltage characteristics for styrene on Si(100)-(2×1). In Sec. V the Tersoff-Hamann approximation is compared with the NEGF results. Section VI is reserved for a short summary.

II. ATOMIC GEOMETRY

We begin by discussing the atomic geometry for three tip-sample systems in our study. The first system is composed of an unrelaxed Al(100) tip above an Al(100) surface [Fig. 1(a)]. This system is used to qualitatively benchmark our STM model. The remaining two systems are hydrogen-passivated Si(100) and styrene on Si(100) [Figs. 1(b) and 1(c)] for which we seek a quantitative understanding of the styrene heights observed experimentally. The atomic structures are obtained by density functional theory (DFT) total energy relaxation using the electronic package SIESTA.[24]

A. Si(100) substrate and STM geometry

To model the STM tip above hydrogen-passivated Si(100) and styrene-passivated Si(100), we have several considerations: tip-sample atomic structure, tip relaxation, positioning of the tip above the sample, and the potential profile through the tip-sample structure that is needed when calculating the tunneling current.

1. Tip and sample structure

To model a metal tip, we use an Al(100)-(3×3) structure with strained coordinates to ensure that the tip geometry embeds into the (7.65 Å×7.65 Å) periodic Si(100)-(2×2) unit cell. The imposed strain on the natural Al(100)-(3×3) unit cell dimensions of (8.57 Å×8.57 Å) is assumed to have an insignificant effect on the metallic tip density of states (DOS) and transmission coefficient, in contrast to covalent-bonded systems where bulk properties can be significantly altered, and is therefore a fair approximation which we adopt. Above silicon a 23-atom tip is placed: the first two bulklike layers are frozen and the remaining five tip atoms are permitted to relax. Two bulk layers are sufficient to model the tip electronic structure, since tip surface states tend to dominate the STM tip transmission coefficient.[25,26]

In experimental measurements[15] on styrene, the STM tip can be placed in direct contact with the molecule; hence, tip-sample geometry relaxation is a key ingredient for obtaining a proper understanding of the measured data. Therefore, we relax the tip above the styrene molecule at each $I(z)$ point, where I is current and z the coordinate along the tip-sample direction. The z values are set at 1-Å intervals. All geometry optimizations are performed via the conjugate gradient method using the local density approximation[24] (LDA)

and are converged to 0.01 eV/Å on a real-space grid corresponding to an energy cutoff of 300 Ry. We find that the relaxed geometry of styrene/Si(100) shown in Fig. 1 is energetically preferred and has a total energy of −2754.768 eV which is lower compared to the total energy (−2754.600 eV) of the alternate styrene chain geometry[27] where the benzene right tilts inwards towards the Si(100) dimer. These energies are rather close, but the one we used is slightly lower.

Careful consideration is taken in the placement of the tip apex atom above the sample. A full image scan within our self-consistent nonequilibrium method (see below) would be too computationally intensive. Instead, the tip is placed above the point of the largest local DOS (LDOS) of the sample and then retracted at a given voltage to build up a current versus distance $I(z)$ plot. In the case of styrene between 0 V and −3 V bias, the highest LDOS point is dominated by carbon-carbon π bonding;[7,15] hence, the tip is placed above the highest carbon atom [see the solid circle in Fig. 1(c)]. Though p orbitals comprising the π state are zero at the carbon orbital core where the LDOS is less than maximum, we have found that the tip-sample overlap coupling changes insignificantly and therefore the extracted STM height as well, if the tip is moved slightly to the side of the uppermost carbon atom where the π orbital LDOS is maximum (see Fig. 7). This is due to the diffuse extent of surface orbitals both on the tip and sample. Hydrogen-passivated Si(100) results in symmetric dimers, so the tip may be placed above either a hydrogen atom or an additional deeper Si atom [see solids circles in Fig. 1(b)].

For each of the three geometries in Fig. 1, the tip is placed 2 Å above the point of interest: this point defines the starting position for subsequent $I(z)$ calculations when the tip is retracted to 10 Å. Due to this definition the 5.3 Å offset between $I(z)$ tip starting positions for H/Si(100) and styrene/Si(100) [Fig. 1(c)] has to be taken into account when comparing $I(z)$ plots to extract the STM heights.

2. Two-probe transport structure

Using the atomic coordinates obtained by total energy relaxation described above, we build a two-probe transport simulation of the tip-sample system for calculating the $I(z)$ curves. The two-probe system has a scattering region plus a top and a bottom lead. The scattering region consists of the atoms in the shaded boxes of Figs. 1(b) and 1(c). Namely, a H/Si(100) or styrene/Si(100) surface, along with a 14-atom tip and four Si(100) layers, is included in the scattering region. The tip is connected to an Al lead that is modeled by perfect Al(100) crystal planes extending to $z=+\infty$. Similarly, the Si substrate in the scattering region is connected to a perfect Si(100) lead extending to $z=-\infty$. Periodic boundary conditions are used in the transverse (x,y) directions. A voltage bias is applied across the two leads which drives a current through the tip-sample two-probe system.

B. Al(100) substrate and STM geometry

An Al(100) tip above an Al(100) substrate is taken as a benchmark of our $I(z)$ calculation (see Sec. III C). For this case the structure is relaxed at a tip-sample separation of 10 Å. No further relaxation is carried out for other values of z. A two-probe tip-substrate system is formed by attaching Al(100) leads for both the tip and substrate. To calculate $I(z)$, the apex atom is placed directly above an aluminum surface atom and retracted [see Figs. 1(a) and 3]. The Al(100) tip-substrate system can be described by the natural Al(100)-(3×3) unit cell size of $(8.57\ \text{Å}\times8.57\ \text{Å})$, the scattering region of the two-probe system includes five tip atoms and five bulk Al layers as shown in Fig. 1(a).

III. THEORETICAL METHOD

When a bias voltage is applied to a two-probe transport structure to drive a current, the scattering region is in a nonequilibrium state. At present, real-space DFT carried out within the Keldysh NEGF framework is the state-of-the-art technique[20,28,29] for analyzing nonequilibrium quantum transport of atomic systems. We make use of this technique and its associated electronic package MATDCAL (Ref. 20) to calculate $I(z)$ curves. The basic idea behind the NEGF-DFT formalism is to calculate the Hamiltonian of a two-probe device system using DFT, determine the nonequilibrium quantum statistics of the transport problem using the NEGF, and deal with the open-boundary conditions of electron transport using real-space numerical techniques.[20,29] We briefly outline our simulation method in this section.

A. Transmission coefficient

Within the NEGF formalism, the transmission coefficient $T=T(E,V)$ is calculated via Green's functions, where E is the electron energy and V the bias voltage. Once the device Hamiltonian H is obtained by NEGF-DFT,[20,29] the retarded Green's function G of the device scattering region at energy E is obtained as

$$G(E)=[(E+i\eta)S-H-\Sigma_S(E)-\Sigma_T(E)]^{-1}, \tag{1}$$

where η is a small positive infinitesimal and S is the overlap matrix between atomic basis functions. The quantities Σ_S and Σ_T are the self-energies of the substrate and STM tip, respectively. They are calculated via recursive Fourier methods.[30,31] The transmission coefficient of a two-probe tip-sample system is determined by

$$T(E,V)=\text{tr}[\Gamma_S G\Gamma_T G^{\dagger}], \tag{2}$$

where $\Gamma_{S,T}=i(\Sigma_{S,T}-\Sigma_{S,T}^{\dagger})$ are the linewidth functions describing coupling of the device scattering region with the semi-infinite device leads. The steady-state current under a given bias is calculated as

$$I=\frac{q}{h}\int_{-\infty}^{\infty}T(E)[f_S(E)-f_T(E)]dE, \tag{3}$$

$$f_{S,T}(E)=\frac{1}{1+e^{(E-\mu_{S,T})/k_BT}}, \tag{4}$$

where $f_{S,T}$ is the Fermi function of the substrate and tip with an electrochemical potential of $\mu_{S,T}$. At low temperature, the

integration limits reduce to the bias window, from μ_S to μ_T. To obtain an $I(z)$ plot, the transmission coefficient $T(E,V)$ and therefore the tip-sample Hamiltonian H must be calculated at many z points.

B. Two-probe device Hamiltonian

In our STM simulation of the $I(z)$ curves, we divide the device Hamiltonian H into two parts: the equilibrium Hamiltonian $\hat{H}_0$ and the nonequilibrium Hartree potential profile $V_{\delta H}(\vec{r})$. The total nonequilibrium Hamiltonian is therefore given by $\hat{H}=\hat{H}_0+V_{\delta H}(\vec{r})$. Here, $\hat{H}_0$ represents the equilibrium Hamiltonian of the tip-sample system without bias, which we calculate within the electronic package SIESTA.[24] The second part of the Hamiltonian, $V_{\delta H}(\vec{r})$, represents the Hartree potential profile between the STM tip and the sample under a three-dimensional applied bias and during current flow; we calculate it via the NEGF-DFT package MATDCAL.[20] We use the generalized gradient approximation (GGA) exchange-correlation potential[32] in $\hat{H}_0$, which improves the Si band gap from 0.5 eV (obtained from LDA[33]) to 0.85 eV.[34]

The nonequilibrium Hartree potential profile $V_{\delta H}(\vec{r})$ is obtained by solving the Poisson equation

$$\nabla^2 V_{\delta H}(\vec{r}) = -4\pi\delta\rho(\vec{r}), \tag{5}$$

where $\delta\rho(\vec{r}) \equiv \rho_{bias}(\vec{r}) - \rho_{eq}(\vec{r})$, ρ_{bias} is the nonequilibrium charge density, and ρ_{eq} the equilibrium charge density; both are obtained by calculating the nonequilibrium density matrix within the NEGF-DFT MATDCAL[20] package.

The calculation of $\hat{H}_0$ is carried out with a 200-Ry energy cutoff. The k-space reciprocal vector for each slab geometry is set at 20 Å.[24,35] We employ double-zeta-polarized (DZP) basis orbitals on hydrogen, carbon, and silicon. For aluminum a single-zeta-polarized (SZP) basis is applied to all atoms. The basis function for the tip apex atom and the surface atom just below the tip will be discussed in the next subsection [see the solid circles in Fig. 1(a)]. The calculation of $V_{\delta H}(\vec{r})$ within MATDCAL[20] in the two-probe tip-sample geometry is carried out on a three-dimensional real-space mesh where the mesh size corresponds to a 150-Ry energy cutoff. Sixteen k points are required to converge the two-dimensional Brillouin zone sampling in the x-y direction (transport in the z direction). To reduce computational time in the two-probe NEGF analysis at finite bias, a SZ basis set is utilized in MATDCAL.[20,36] The NEGF-DFT analysis via MATDCAL[20] provides the potential drop between the tip and substrate within a full self-consistent framework at different tip-sample distances and bias voltages. Further details of the NEGF-DFT implementation can be found in Refs. 20 and 29.

C. Basis set

For a two-probe tip-sample system, the value of the tunneling current $I(z)$ is sensitive to the wave-function overlap between the surface and tip across the vacuum in between. This becomes a technical issue when a strongly localized linear combination of atomic orbitals (LCAO) basis set[24] is used in the DFT analysis. It is reasonable to assume that the atom at the tip apex and atoms at the surface have the same character of wave function decay into the vacuum as that of a free isolated atom: these wave functions are valence electron eigenfunctions of isolated atoms having a long-range tail decaying into the vacuum region. In our calculations, we assign these free atomic orbitals as basis functions to the tip apex atom and atoms at the surface beneath the tip. Practically, we generate free atomic orbitals following the approach of Ref. 37, using a large radial cutoff of 15 bohrs. The secondary split-off orbitals[24,37,38] are defined at 5 bohrs as are polarization orbitals. These parameters are the same for all free atomic orbitals implemented in this work with results comparable to those in an earlier publication.[40]

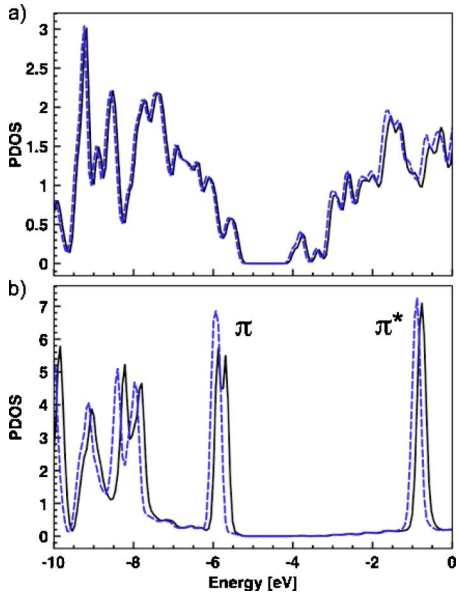

FIG. 2. (Color online) PDOS for the Si(100)-(2×2) unit cell. Dashed line: calculated with free atomic orbitals placed as shown by the red dots in Fig. 1. Solid line: calculated without the free orbitals. (a) For the first layer of silicon atoms and hydrogens on H-passivated Si(100). (b) For styrene on Si(100). The agreement is reasonable with or without the free atomic orbitals. Similar agreement (not shown) is found for the case of Al(100) substrate.

The free atomic orbitals introduce some error into the eigenstates and the total energy. To minimize this error, no more than two or three free atomic orbitals are assigned to any given unit cell (see Fig. 1): one for the tip apex atom and a second or third (if necessary) for the sample atoms beneath the tip—no more is required as these atoms dominate the $I(z)$ characteristics. Figure 2 displays the effect of introducing free atomic orbitals to the Si(100)-(2×2) surface atoms highlighted by solid circles in Fig. 1, against reference calculations employing optimized DZP basis sets without any free orbitals. The projected density of states (PDOS) plots are extracted from isolated H/Si(100) and styrene/Si(100) slabs shown in Fig. 1. For H/Si(100) the PDOS shift is about 0.1 eV; for styrene it is about 0.25 eV. With a free atomic orbital the styrene system has a total energy of −4155.85 eV, to be compared to −4155.67 eV when free orbitals are absent. With free orbitals the H/Si(100) system has a total energy of −2778.71 eV, to be compared with −2778.94 eV without it. These are very small differences, indicating that

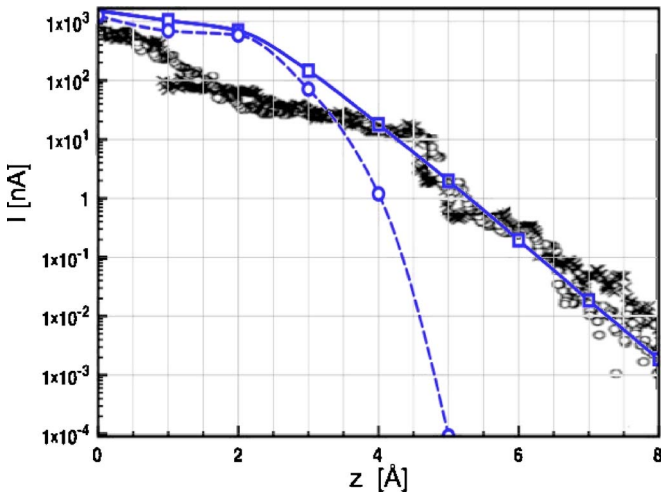

FIG. 3. (Color online) $I=I(z)$ versus z for Al tip on Al(100) at 50 meV bias for $E_f=-4$ eV. Solid line: using free atomic orbitals. Dashed line: using SZP with 7-bohr cutoff. Symbols × are experimental data reprinted with permission from Ref. 39. The offset for the experimental data is −0.8 Å from the origin provided in Ref. 39 since the nearest-neighbor distance of Al is 2.86 Å and the above $I(z)$, as with all plots in this paper, sets its origin at a 2-Å atomic separation.

the use of a few free atomic orbitals only introduces an insignificant error for the purposes of our investigation. In subsequent simulations, we use free atomic orbitals on the tip apex atom and the substrate atoms of interest.

We find that the above procedure succeeds well in modeling STM current decay, as shown in Fig. 3 where a qualitative match to experimental decay is achieved. Here, the $I(z)$ curve is calculated for an Al(100) tip and an Al(100) substrate biased at $V=50$ meV (solid line). For such a very small bias we have safely neglected the nonequilibrium potential $V_{\delta H}(\vec{r})$ of Eq. (5) in the transmission calculation. Compare this to the $I(z)$ curve obtained without using free atomic orbitals (dashed line); it decays much faster in an unphysical manner as shown in Fig. 3.

To have a more concrete understanding, in Fig. 3 we also plot experimental data in the same z range from Ref. 39, where the tip is tungsten and substrate is Au(111)-(22 $\times\sqrt{3}$). The work functions of Au and W are[41] −5.31 eV and −4.45 eV, respectively, and for Al(100) it is −4.2 eV. These values can be used in a simple square barrier STM model[42] to estimate how much difference we expect in the current decay for the Al/Al system (our theory) and for the W/Au system (experiment). In a square barrier model,[41] the current decays exponentially with z,

$$I = I_0 e^{-1.025\sqrt{\phi}z}, \tag{6}$$

where z is in units of Å, ϕ is the work function in units of eV, and I_0 is assumed to be the same for both systems. From Eq. (6), we find that the $I(z)$ decay expected from the experimental system should not exceed that of the simulated Al(100) geometry by more than ~0.11 decibel/Å, assuming an experimental work function of −5.31 eV. Indeed, the theoretical result (solid line) in Fig. 3 shows a decay rate close to that of the experimental data (a qualitative difference of 0.11 decibel/Å is within the bounds of experimental error), indicating that the procedure of using free atomic orbitals is appropriate. The long-range $I(z)$ decay of 1 decibel/Å also agrees well with that observed for an Al surface and W tip.[43]

This comparison between theory and experiment underscores the necessity of applying free atomic orbitals when modeling long-range $I(z)$ decay. In the near range, below 3.0 Å where relaxation effects become important, contracted and free orbitals decay in almost exactly the same manner (for a typical bulk cutoff radius of 7 bohrs). Whether a fully relaxed geometry is applied to a STM study or not, free and contracted atomic orbitals will produce the same $I(z)$ currents in the near-range. Hence, near-range surface relaxation is irrelevant to the question as to what basis-set cutoff radius should be used to model tunneling currents in the vacuum region and has therefore been excluded from this Al-Al study.

IV. STYRENE IMAGE HEIGHTS ON Si(100)

Using the theoretical technique discussed in Sec. III, we have calculated the STM image height of styrene on hydrogen passivated Si(100). Three bias voltages at 50 pA current are examined in detail: −3 V where the π state is fully conducting, −2 V where the π state begins to conduct, and −1.2 V where height inversion is observed.[2,15,16] We quantitatively analyze the role of the nonequilibrium potential profile $V_{\delta H}(\vec{r})$ and the band gap in determining STM heights.

As mentioned above, for atoms just across (facing) the vacuum gap we assign free orbitals. Specifically, we assign a free atomic orbital to the apex atom of the Al(100) tip (see apex solid circle in Fig. 1). For hydrogen-passivated Si(100), DZP free atomic orbitals are placed sparingly on one Si-H surface pair in the simulated (2×2) unit cell [Fig. 1(c)]. Because occupied surface states involve strong hybridization between the hydrogen and silicon atoms, free atomic orbitals are placed on two atoms [solid circles in Fig. 1(c)]. On the other hand, the conducting π state of styrene centered at −6 eV [see Fig. 2(b)] is much more weakly hybridized, as well the π state being composed of carbon-carbon bonding.[15] Thus, a single free atomic orbital is placed on the highest carbon atom over which the tip is positioned [see the solid circle in Fig. 1(c)]. For the bias range of interest conduction is completely dominated by the styrene π state; therefore, it is sufficient to place a free orbital on the uppermost carbon atom. Our calculation also indicates that image heights are not affected if a free atomic orbital is also placed on the uppermost hydrogen atom. However, additional free orbitals increase the eigenstate error and are therefore minimized.

A. Styrene at −3.0 V: Full π-state conduction

Simulated and experimental heights match well for styrene biased at −3 V and 50 pA [see Fig. 4(a)]. The experimentally measured styrene height is approximately 3.3 Å at 60 pA.[2,16] Our calculation gives 3.4 Å at 50 pA which is in good agreement. This 3.4 Å result is obtained as follows. The $I=50$ pA line (horizontal dot-dashed line) in Fig. 4(a)

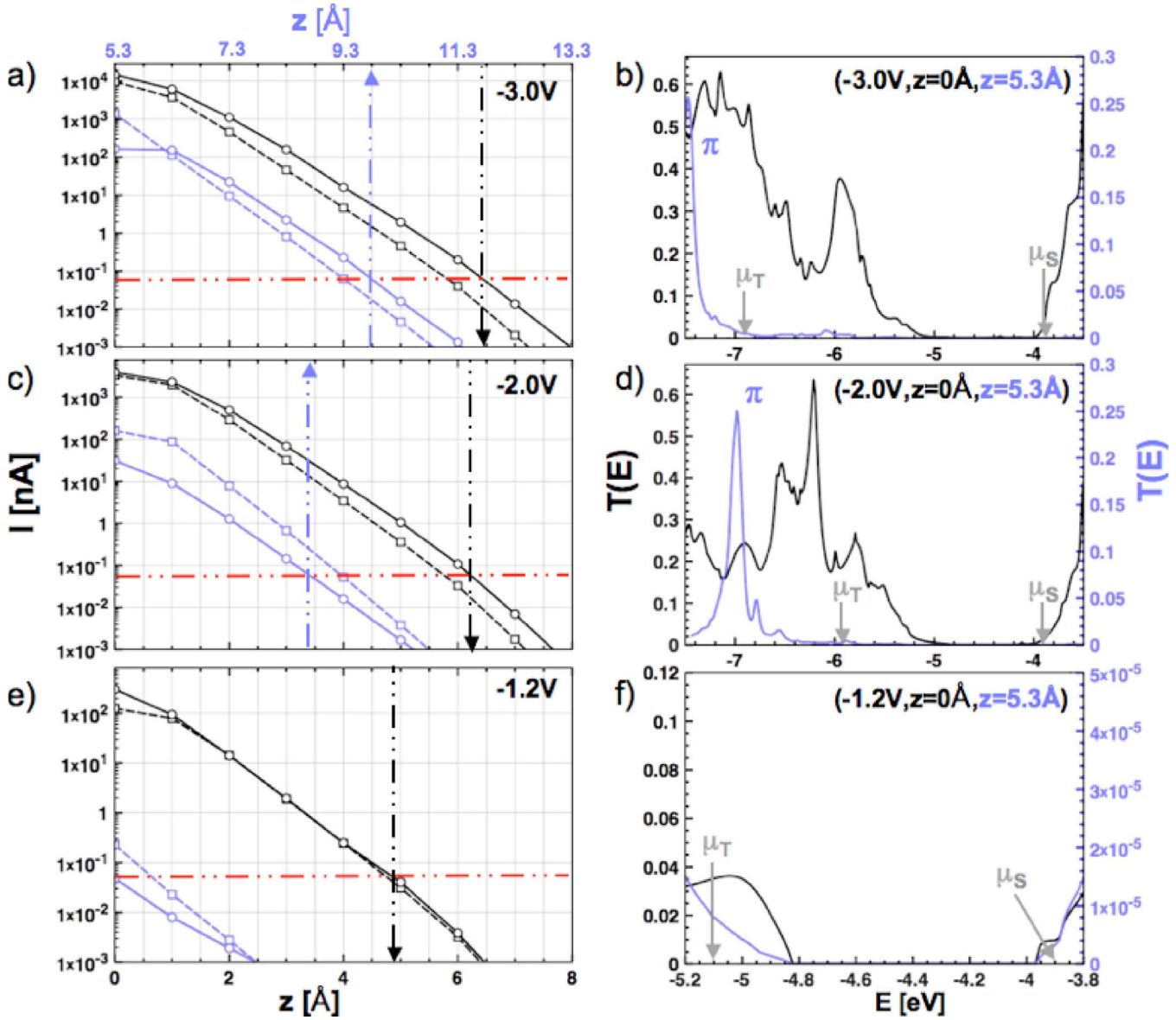

FIG. 4. (Color online) $I(z)$ characteristics for H/Si(100) in black (equilibrium, dashed line, and nonequilibrium, solid line) and styrene in blue at (a) −3 V bias, (c) −2 V bias, and (e) −1.2 V bias. The experimental current value of 50 pA is marked by dashed horizontal red lines. Equilibrium $I(z)$ results are obtained by calculating the transmission between both electrochemical potentials without including a potential drop in the device region, whereas nonequilibrium results include the self-consistent potential profile $V_{\delta H}(\vec{r})$. Nonequilibrium transmission plots may be found adjacent to each $I(z)$ figure with H/Si(100) in black and styrene in blue (in each plot the tip is positioned 2 Å above the sample at full bonding contact): (b) −3 V, η=10 meV; (d) −2 V, η=10 meV; (f) −1.5 V, η=1 μeV. Recall that η is defined in Eq. (1) as a broadening constant for the retarded Green's function of the device. The universal $I(z)$ origin is set at 2 Å above the core of the hydrogen atom on the hydrogen passivated Si(100) surface marked in Fig. 1. The upper blue z axis is for the styrene $I(z)$ curves and the lower back z axis is for the hydrogen passivation $I(z)$ curves as indicated by the dashed colored arrows. Relaxation is included in the styrene $I(z)$ plots. The π state for styrene is marked in the transmission plots as are the electrochemical potentials μ_T and μ_S, respectively.

cuts the two $I(z)$ curves (solid lines) at z_H=6.4 Å for H/Si and at $z_{styrene}$=9.8 Å for styrene (for the hydrogen passivation tip position look to the lower black z axis and for the styrene tip position look to the upper blue z axis in Fig. 4). The apparent height of styrene at 50 pA is obtained by subtracting the difference such that $z_{styrene}-z_H$=3.4 Å. The two solid $I(z)$ curves in Fig. 4 further suggest that raising the set current from 50 pA to 60 pA changes the styrene height measurement insignificantly. The agreement between theory and experiment height values at (−3 V, 50 pA) is, indeed, remarkable. It is also worth noting that the $I(z)$ current decay of approximately 1 decibel/Å over both H/Si(100) and styrene is consistent with experimental measurements over cyclopentene-passivated Si(100).[44]

The small height difference of ~0.1 Å between our calculation and experimental data[16] is likely due to subtle polarization effects or due to the approximation of using free atomic orbitals. In the literature there has been some disagreement of styrene heights on hydrogen-passivated Si(100) at −3 V, with measured heights ranging from 2.8 Å[15] to

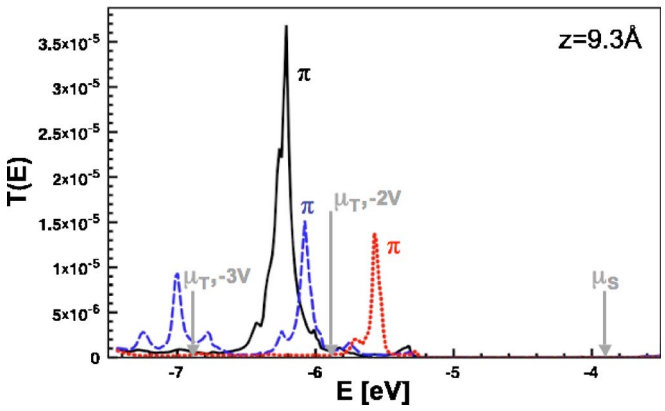

FIG. 5. (Color online) Transmission coefficient $T(E)$ versus electron energy E when the tip is positioned 6 Å above the styrene molecule (in relation to the universal origin set at 2 Å above H/Si of Fig. 4 this corresponds to z=9.3) in Fig. 4 for styrene biased at −3 V (solid black line) and −2 V (dashed blue line). Nonequilibrium potential drop $V_{\delta H}(\vec{r})$ is included when obtaining these curves. The dotted red line is $T(E)$ without $V_{\delta H}(\vec{r})$. The peaks in $T(E)$ are due to the molecular π state of styrene. At −3 V bias, the π state is within the bias window indicated by arrows of $\mu_{S,T}$. At −2 V bias, it is outside the bias window due to the nonequilibrium potential drop $V_{\delta H}(\vec{r})$. The peak of $T(E)$ at −3 V is much larger than that at −2 V due to a decrease in the vacuum barrier under a larger bias.

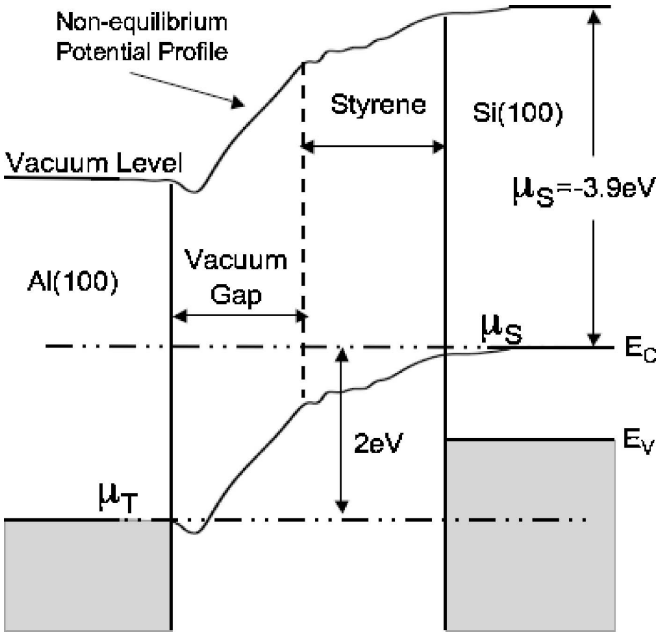

FIG. 6. Calculated nonequilibrium potential profile at −2 V bias for a styrene molecule situated between a grounded tip and Si(100) substrate (see Fig. 1). The potential profile shown is taken as a z direction cut directly through the atomic center of the tip apex. The Si(100) electrochemical potential μ_S is set at −3.9 eV, corresponding to a highly n-doped substrate and with the reference vacuum potential set at 0 eV. Under a −2 V bias the tip electrochemical potential $\mu_T=\mu_S-2$ eV=−5.9 eV. Most of the potential drops across the vacuum region, with roughly one-third of the potential dropping across the styrene molecule—a ratio that depends on the size of the vacuum region. Similar results can be obtained via a simple capacitive model (Ref. 9).

3.3 Å,[2,16] which could be due to a slight variation in the point over which height measurements were taken. More recently, it has been observed that measurements at (−3.0 V, 50 pA) to one side of the styrene chain give a reduced height of 3.1 Å.[16] In our results reported here, all $I(z)$ curves are calculated by placing the tip apex just above the highest carbon atom of the carbon ring.

In Fig. 4(a), the two dashed $I(z)$ curves were obtained without the nonequilibrium potential profile $V_{\delta H}(\vec{r})$ of Eq. (5); namely they are calculated at equilibrium. For both styrene and H/Si, $V_{\delta H}(\vec{r})$ increases the tunneling current. Using these dashed $I(z)$ curves, we still obtain a similar styrene height as the full nonequilibrium calculation (differs by only 0.2 Å). Therefore, at −3 V, the main role of the nonequilibrium potential $V_{\delta H}(\vec{r})$ is to lower the vacuum barrier and increase the current [compare dashed and solid lines in Fig. 4(a)]. In particular, due to $V_{\delta H}(\vec{r})$, the styrene tip-sample distance increases by ~0.5 Å at (−3 V, 50 pA), compared with that obtained with the equilibrium Hamiltonian. For tunneling into H/Si, there is a similar although slightly larger increase in current when $V_{\delta H}(\vec{r})$ is included; see Fig. 4(a).

For a given bias $V=\mu_S-\mu_T$, current is contributed by states within the bias window $\mu_S-\mu_T$ [see Eq. (3)]. Tunneling into styrene is largely mediated by the molecular π state; therefore, it is important if the π state is within this bias window or not. In our calculations, μ_S is set at the Fermi level of the n^{++}-doped Si contacts—namely, at −3.9 eV[41,45]—and μ_T is shifted by the applied bias voltage. Figure 4(b) plots the transmission coefficient $T(E)$ at −3 V bias when the tip apex is at 2 Å away from the highest atom on the sample; $\mu_{S,T}$ are indicated by the arrows. Figure 4(b) shows that the π state of styrene is outside the bias window whereas for H/Si the transmission has a broad peak inside the bias window. On the other hand, for z=9.3 Å (the tip apex is at 6 Å from the styrene molecule), the styrene π state is within a bias window of −3 V, as shown by the solid curve in Fig. 5 (see also Fig. 6). Importantly, the π state is within the bias window whether or not the nonequilibrium potential $V_{\delta H}(\vec{r})$ is included in our calculation. This explains why the styrene height at (−3 V, 50 pA) can be rather well obtained using only the equilibrium Hamiltonian without $V_{\delta H}(\vec{r})$. In the next subsection, we show that the height behavior becomes very different depending on $V_{\delta H}(\vec{r})$.

B. Styrene at −2.0 V: Lowering the conducting π state

The $I(z)$ curves for (−2 V, 50 pA) are plotted in Fig. 4(c). Here, for tunneling into H/Si the nonequilibrium potential $V_{\delta H}(\vec{r})$ still increases current $I(z)$ as at −3 V. However, for styrene the behavior is reversed: $V_{\delta H}(\vec{r})$ decreases the current. The reason for this decrease can be seen in Fig. 5: the styrene π state (dashed line) is now outside the bias window between μ_S=−3.9 eV and $\mu_T=(\mu_S-2\text{ eV})$=−5.9 eV due to $V_{\delta H}(\vec{r})$. It is, however, inside the window without $V_{\delta H}(\vec{r})$ (dotted line). Pulling the π state outside the bias window by $V_{\delta H}(\vec{r})$ results in a net decrease of 0.6 Å between the equilibrium and nonequilibrium results at 50 pA. The total height

correction due to $V_{\delta H}(\vec{r})$ over both styrene and H/Si(100) is about 1 Å. Therefore, using the method for height calculation described at the beginning of Sec. IV A, from the two $I(z)$ curves (solid lines) in Fig. 4(c) we obtain a styrene height of 2.5 Å for (−2 V, 50 pA). This is to be compared with the experimental value of 2.6 Å at (−2 V, 60 pA).[2,16] Again, we compare results against experimental styrene heights away from the ends of an adsorbed chain, and the agreement is very good. Importantly, the effect of $V_{\delta H}(\vec{r})$ is very crucial at −2 V: it places the STM tip closer to the styrene than would be estimated using the equilibrium Hamiltonian. Again, due to a reduction of the vacuum barrier, we note an increase in the H/Si(100) tip-sample distance of approximately 0.6 Å over that predicted by the equilibrium Hamiltonian. Finally, Fig. 4(d) plots $T(E)$ at tip-sample separations 2 Å above H/Si and styrene and qualitative features are similar to that of Fig. 4(b).

C. Styrene at −1.2 V: The height inversion

Figure 4(e) plots $I(z)$ curves for (−1.2 V, 50 pA) showing a styrene height inversion; i.e., styrene (almost) appears lower than H/Si(100). This is consistent with the experimental trend of height inversion observed at (−1.5 V, 50 pA).[16] The difference of −0.3 V bias may be attributed to an underestimation of the Si band gap in our DFT calculations: our DFT-GGA calculation gives[32] a gap of 0.85 eV while the experimental gap is 1.15 eV. Therefore, the height inversion at −1.2 V obtained from our model compares well with the experimental observation of height inversion at −1.5 V.

Contrary to expectations, we find that a tip-sample bonding interaction is *not* responsible for the observed styrene height inversion. This is because, at lower bias voltages, it is the band gap which determines STM transmission characteristics. Figure 4(f) demonstrates this feature: at −1.2 V bias the main part of the $T(E)$ spectra falls within the Si band gap, thus not contributing to conduction, leaving only a small surface DOS at the edges of the band gap to contribute. This leads to a drastic reduction in current flow through styrene at this bias, resulting in the observed height inversion.

Quantitatively, for (−1.5 V, 50 pA) the experimental height is reported to range from −0.25 Å to 0 Å in an STM image of several styrene chains.[15] Using the height calculation method described at the beginning of Sec. IV A, our theory gives 0.4 Å at (−1.2 V, 50 pA). Therefore, although the theoretical height is drastically reduced which mimics the qualitative feature of height inversion of the measurement, it does not quantitatively capture the experimental inversion value with a small error of about one-third of an angstrom. The source of this error is unlikely to be related to the geometry because it was carefully relaxed for each value of z. We hypothesize that the error is due to the details of DFT: the conduction and valance band curvatures are reflected in the surface LDOS which contributes to conduction, with lower curvature resulting in a larger surface LDOS and vice versa.[11] This curvature depends on the DFT basis set. Nevertheless, qualitatively and even semiquantitatively, our theory reproduces the height inversion feature of the experimental data.

D. Bonding distance

Now let us return to the question of a bonding contact between an atomic sample and a STM tip as posed in the Introduction. There are two main physical effects which limit the full current at full contact: the resistance of the molecule and the Si(100) band gap. The molecule impedes conduction from bulk Si(100) states and lowers the current by approximately two orders of magnitude at −3 V and −2 V, as shown in Figs. 4(a) and 4(b) when the tip is located at $z=0$ Å over H/Si and $z=5.3$ Å over styrene (recall $z=0$ is positioned 2 Å above the H/Si surface). Notably, at full contact the styrene π state is pulled out of the bias window even at −3 V bias [see Fig. 4(b)], hence the observed insulating type of resistance. At full contact, if a level lines up between the chemical potentials $\mu_{S,T}$, conductance will be high; otherwise, the molecule conducts poorly. At −1.2 V, the low LDOS of styrene in the bias window together with the Si(100) band gap affects conduction such that the current is four orders of magnitude smaller than that on H/Si(100). Our observation is that an Al tip placed at 2 Å bonding distance above either H/Si(100) or a styrene molecule forms a physisorption bond. This is confirmed by a charge density plot of the tip-sample interface (not shown). Thus, the lack of a strong chemical bond between styrene and the STM tip does not play a role in the observed decrease in conduction from H/Si(100) to styrene—since the tip also forms a weak physisorption bond with the H/Si(100) surface. Further investigation into chemical bonding versus physisorption bonding conduction characteristics is left to future work, and other metallic tips such as tungsten should be investigated. However, here it has been shown that even current at full contact depends strongly on the presence of a bulk band gap and the conducting resonance properties of the molecule, and may vary significantly with only a small change in bias (i.e., −1.2 V to −2 V). Our full self-consistent NEGF-DFT theory presented here captures these complicated effects.

E. Si(100) band bending

Silicon band bending[46] is another important issue which has not been considered so far. For our problem studied here, it is found to have little effect on transmission: it only provides a maximum shift of surface states about 0.1 eV at room temperature and negative STM bias[45] for n-type doping on the order of 10^{18} cm^{-3}. Band bending could shift surface states by 0.01–0.1 eV without altering the qualitative features presented above. That is, the characteristics seen at −3 V would be better matched to experimental results at −3.1 V, etc. Even n-type doping on the order of 10^{16} cm^{-3} would only result in a 0.2-eV shift of surface states at room temperature. A proper treatment of band bending within a true *ab initio* methodology is beyond the scope of this work.[47] As a final remark, in this analysis we have excluded effects of electric field polarization, since strong polarization is so far known to be limited to clean silicon[7,8] whereas this work is focused on H-passivated Si(100).

V. COMPARISON TO THE TERSOFF-HAMANN APPROXIMATION

So far our results have been obtained via the self-consistent NEGF theory discussed in Sec. III. In the follow-

ing section we calculate STM heights by the Tersoff-Hamann (TH) approximation[23] and compare the TH results to the NEGF results shown in the previous section. We begin by manipulating Eq. (2) as follows:

$$T = \mathrm{tr}[\Gamma_S G \Gamma_T G^\dagger] = \mathrm{tr}[\tau_S A_S \tau_S^\dagger G \tau_T^\dagger A_T \tau_T G^\dagger]$$
$$= \mathrm{tr}[A_S \tau_S^\dagger G \tau_T^\dagger A_T \tau_T G^\dagger \tau_S] = \mathrm{tr}[A_S M A_T M^\dagger], \quad (7)$$

where G is the Green's function of the scattering region, τ_S and τ_T are couplings of this region to the semi-infinite substrate and tip, and M represents coupling between the left and right contact spectral functions A_T and A_S.[28] If the coupling is weak, we may take M to be a constant. If the DOS in the metallic STM tip is relatively flat such that A_T may be approximated by a constant, one obtains an approximate transmission coefficient: namely, the TH approximation

$$T(E, \vec{r}_0) \propto \mathrm{tr}[A_S(E, \vec{r}_0)] = \rho_S(E, \vec{r}_0), \quad (8)$$

where A_S is in an orthogonal basis. Therefore, in the TH approximation the tunneling current is determined by the LDOS $\rho_S(E, \vec{r}_0)$ of the sample at the tip apex position $\vec{r}_0$. The approximation involved in arriving at Eq. (8) dictates that the TH approximation is valid for STM height simulations in the strong tunneling limit and it breaks down when tip-sample interactions are important. The larger the distance between the tip and sample, the better the TH approximation.

In practical calculations using Eq. (8), electronic structures of the tip and sample are taken to be independent from each other and any tip-sample interaction is neglected. We chose to compute image heights at −3 V, because among the three voltages analyzed in Sec. IV, this case presents the largest distance between styrene and the tip at 50 pA. Figure 7 shows a height scan obtained by the TH method at (−3 V, 50 pA) where the separation between the highest styrene atom and the tip apex is 6.5 Å. In order to maintain consistency when comparing the TH approximation to the NEGF result of Sec. IV, we have kept the same placement of free atomic orbitals shown in Fig. 1 and other DFT details. We find that the STM styrene height obtained by the TH method differs from the experimental value by about 1.0 Å [this has been independently confirmed in an ABINIT (Ref. 48) plane-wave TH calculation]. This large difference is unlikely due to effects of the applied tip-sample electric field, because at (−3 V, 50 pA), the NEGF results in Sec. IV A show that there is little difference in the calculated equilibrium and nonequilibrium styrene heights [they differ by only 0.2 Å; see Fig. 4(a) and discussions in Sec. IV A]. Therefore we attribute this difference to the electronic coupling between the tip and sample[49] which has been neglected in the TH approximation in the large bias range of −3 V.

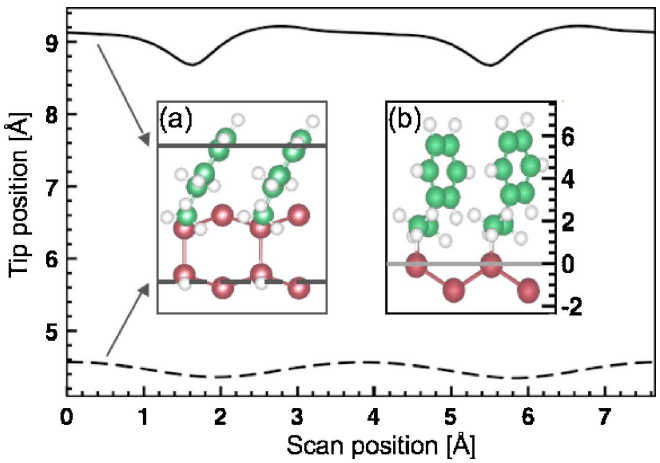

FIG. 7. (Color online) STM height scan at (−3 V, 50 pA) calculated within the Tersoff-Hamann approximation. The data are extracted from the bias window of $\mu_S = -3.9$ eV to $\mu_T = \mu_S - 3$ eV $= -6.9$ eV at a constant electron density contour of 10^{-5} e/bohr^3. Dashed line: taken over the maximum height of H-passivated Si(100) surface. Solid line: taken over the maximum height of a styrene chain where the π state is clearly indicated by the two large dips in the curve. The height difference is 4.5 Å, which is about 1 Å larger than that obtained by NEGF theory. Inset (a): showing orientation and position of the styrene and hydrogen Si(100) LDOS scans looking down on the Si(100) surface. Inset (b): a side view showing the origin of the tip position relative to the molecular heights. Note that the origin assigned here is unrelated to those taken in the $I(z)$ plots in the other figures.

VI. SUMMARY

We have calculated the STM image heights of styrene on Si(100) using density functional theory within the Keldysh nonequilibrium Green's function formalism. The nonequilibrium potential drop between Si(100) and a STM tip is determined self-consistently and is found to play an important role in the calculated image heights. The nonequilibrium potential profile affects STM heights by shifting resonant molecular levels out of the bias window and by lowering the vacuum barrier. The presence of a bulk Si band gap is found to play a crucial role in observed molecular height inversion at low imaging voltages. Our NEGF formalism correctly and quantitatively captures STM heights of styrene on Si(100) as compared to experimental data. Our numerical results also provide a microscopic physical picture behind the height characteristics including the height inversion. However, it should be noted that the DFT general gradient approximation may introduce an error into the calculated styrene π state energetic position on Si(100) which could be reconciled by more sophisticated GW calculations.[19] As well our analysis includes an aluminum tip, whereas the experimental measurements employ a tungsten tip. We also present a comparison between results obtained by the NEGF-DFT formalism and the Tersoff-Hamann approximation, showing that nonequilibrium analysis can be important in the study of the STM image heights of molecules.

ACKNOWLEDGMENTS

We gratefully acknowledge financial support from ARODURINT and the NSF Network for Computational Nanotechnology (Purdue), NSERC of Canada, FRQNT of Quebec, and CIAR (McGill). We thank D. Waldron for his kind help with the MATDCAL software package used in this work.

*kbevan@purdue.edu.

[1] G. V. Nazin, X. H. Qiu, and W. Ho, Phys. Rev. Lett. **90**, 216110 (2003).
[2] P. Piva, G. A. DiLabio, J. L. Pitters, J. Zikovsky, M. Rezeq, S. Dogel, W. A. Hofer, and R. A. Wolkow, Nature (London) **435**, 658 (2005).
[3] N. P. Guisinger, M. E. Greene, R. Basu, A. S. Baluch, and M. C. Hersam, Nano Lett. **4**, 55 (2004).
[4] P. Zhang, E. Tevaarwerk, B. Park, D. E. Savage, G. K. Celler, I. Knezevic, P. G. Evans, M. A. Eriksson, and M. G. Lagally, Nature (London) **439**, 703 (2006).
[5] M. Lastapis, M. Martin, D. Riedel, L. Hellner, G. Comtet, and G. Dujardin, Science **308**, 1000 (2005).
[6] N. P. Guisinger, N. L. Yoder, and M. C. Hersam, Proc. Natl. Acad. Sci. U.S.A. **102**, 8838 (2005).
[7] H. Ness and A. J. Fisher, Phys. Rev. B **55**, 10081 (1997).
[8] H. Ness, A. J. Fisher, and G. A. D. Briggs, Surf. Sci. **380**, L479 (1997).
[9] T. Rakshit, G. C. Liang, A. W. Ghosh, M. C. Hersam, and S. Datta, Phys. Rev. B **72**, 125305 (2005).
[10] G. C. Liang and A. W. Ghosh, Phys. Rev. Lett. **95**, 076403 (2005).
[11] D. Kienle, K. H. Bevan, G. Liang, L. Siddiqui, J. I. Cerdá, and A. W. Ghosh, J. Appl. Phys. **100**, 043715 (2006).
[12] A. J. Mayne, A. R. Avery, J. Knall, T. S. Jones, G. A. D. Briggs, and W. H. Weinberg, Surf. Sci. **284**, 247 (1993).
[13] W. A. Hofer, A. J. Fisher, and R. A. Wolkow, Surf. Sci. **475**, 83 (2001).
[14] W. Kim, H. Kim, G. Lee, Y. K. Hong, K. Lee, C. Hwang, D. H. Kim, and J. Y. Koo, Phys. Rev. B **64**, 193313 (2001).
[15] W. A. Hofer, A. J. Fisher, G. P. Lopinski, and R. A. Wolkow, Chem. Phys. Lett. **365**, 129 (2002).
[16] G. Kirczenow, P. G. Piva, and R. A. Wolkow, Phys. Rev. B **72**, 245306 (2005).
[17] G. P. Lopinski, T. M. Fortier, D. J. Moffatt, and R. A. Wolkow, J. Vac. Sci. Technol. A **16**, 1037 (1998).
[18] P. A. Sloan and R. E. Palmer, Nature (London) **434**, 367 (2005).
[19] G. M. Rignanese, X. Blase, and S. G. Louie, Phys. Rev. Lett. **86**, 2110 (2001).
[20] D. Waldron, P. Haney, B. Larade, A. MacDonald, and H. Guo, Phys. Rev. Lett. **96**, 166804 (2006) and references therein.
[21] P. S. Damle, A. W. Ghosh, and S. Datta, Phys. Rev. B **64**, 201403(R) (2001).
[22] W. A. Hofer, A. S. Foster, and A. L. Shluger, Rev. Mod. Phys. **75**, 1287 (2003).
[23] J. Tersoff and D. R. Hamann, Phys. Rev. B **31**, 805 (1985).
[24] J. M. Soler, E. Artacho, J. D. Gale, A. García, J. Junquera, P. Ordejón, and D. Sánchez-Portal, J. Phys.: Condens. Matter **14**, 2745 (2002).
[25] P. A. Sloan and R. E. Palmer, Nano Lett. **5**, 835 (2005).
[26] P. Sutter, P. Zahl, E. Sutter, and J. E. Bernard, Phys. Rev. Lett. **90**, 166101 (2003).
[27] J.-H. Cho, D.-H. Oh, and L. Kleinman, Phys. Rev. B **65**, 081310(R) (2002).
[28] S. Datta, *Quantum Transport: Atom to Transistor* (Cambridge University Press, Cambridge, UK, 2005).
[29] Jeremy Taylor, Hong Guo, and Jian Wang, Phys. Rev. B **63**, 245407 (2001).
[30] M. P. Lopéz Sancho, J. M. Lopéz Sancho, and J. Rubio, J. Phys. F: Met. Phys. **15**, 851 (1985).
[31] F. Zahid, M. Paulsson, and S. Datta, in *Advanced Semiconductors and Organic Nano-techniques (III)*, edited by H. Morkoc (Academic Press, Burlington, MA, 2003).
[32] I. H. Lee and R. M. Martin, Phys. Rev. B **56**, 7197 (1997).
[33] M. Rohlfing, P. Krüger, and J. Pollmann, Phys. Rev. B **52**, 1905 (1995).
[34] At present, only the LDA is implemented in the NEGF-DFT package MATDCAL (Ref. 20) for the two-probe geometry. Splitting the Hamiltonian this way allows one to access the GGA exchange-correlation potential of SIESTA (Ref. 24). This approximation neglects some small corrections to the exchange-correlation potential due to finite bias. This is acceptable because of the small bias range used in this work.
[35] J. Moreno and J. M. Soler, Phys. Rev. B **45**, 13891 (1992).
[36] O. F. Sankey and D. J. Niklewski, Phys. Rev. B **40**, 3979 (1989).
[37] J. Junquera, O. Paz, D. Sanchez-Portal, and E. Artacho, Phys. Rev. B **64**, 235111 (2001).
[38] J. Cerdá, A. Yoon, M. A. Van Hove, P. Sautet, M. Salmeron, and G. A. Somorjai, Phys. Rev. B **56**, 15900 (1997).
[39] Y. Sun, H. Mortensen, S. Schär, A. S. Lucier, Y. Miyahara, P. Grütter, and W. Hofer, Phys. Rev. B **71**, 193407 (2005).
[40] J. M. Blanco, C. Gonzalez, P. Jelinek, J. Ortega, F. Flores, and R. Perez, Phys. Rev. B **70**, 085405 (2004).
[41] *CRC Handbook of Chemistry and Physics* (CRC Press, New York, 2003).
[42] C. J. Chen, *Introduction to Scanning Tunneling Microscopy*, Oxford Science Publications (Oxford University Press, Oxford, 1993).
[43] J. Wintterlin, J. Wiechers, H. Brune, T. Gritsch, H. Höfer, and R. J. Behm, Phys. Rev. Lett. **62**, 59 (1989).
[44] R. Akiyama, T. Matsumoto, and T. Kawai, Phys. Rev. B **62**, 2034 (2000).
[45] R. F. Pierret, *Advanced Semiconductor Fundamentals*, 2nd edition (Prentice-Hall, Upper Saddle River, NJ, 2002).
[46] M. McEllistrem, G. Haase, D. Chen, and R. J. Hamers, Phys. Rev. Lett. **70**, 2471 (1993).
[47] L. Liu, D. Waldron, and H. Guo, in *Proceedings of the 2006 8th International Conference on Solid-State and Integrated Circuit Technology, Shanghai, China, 2006*, edited by Ting-Ao Tang, Guo-Ping Ru, and Yu-Lnog Jiang (IEEE Press, Englewood Cliffs, NJ), p. 1411.
[48] X. Gonze, J. M. Beukena, R. Caracasa, F. Detrauxa, M. Fuchsa, G. M. Rignanesea, L. Sindica, M. Verstraetea, G. Zerahb, F. Jolletb, M. Torrentb, A. Royb, M. Mikamic, Ph. Ghosezd, J. Y. Ratyd, and D. C. Allane, Comput. Mater. Sci. **25**, 478 (2002).
[49] W. A. Hofer, J. Redinger, A. Biedermann, and P. Varga, Surf. Sci. Lett. **466**, L795 (2000).